Trilobatin attenuates cerebral ischemia/reperfusion-induced blood-brain-barrier dysfunction by targeting MMP9: The legend of a food additive

Linying Feng[1], Yeli Li[1], Mu Lin [1], Dianyou Xie[1], Yunmei Luo[1], Zhi-Xu He[2], Qihai Gong[2], zhu yizhun[1], and Jianmei Gao[2]

[1]Macau University of Science and Technology
[2]Zunyi Medical University

February 15, 2023

Abstract

Background and Purpose: Blood-brain barrier (BBB) breakdown is one of the most crucial pathological changes of cerebral ischemia-reperfusion (I/R) injury. Trilobatin (TLB), a naturally occurring food additive, exerts neuroprotective effect against cerebral I/R injury as demonstrated in our previous study. This study was designed to investigate the effect of TLB on disruption of BBB after cerebral I/R injury. Experimental Approach: Rats with focal cerebral ischemia caused by transient middle cerebral artery occlusion (MCAO) and brain microvascular endothelial cells along with human astrocytes to mimic blood brain barrier (BBB) injury caused by oxygen and glucose deprivation (OGD) followed by reoxygenation (OGD/R). Key results: The results showed that TLB effectively maintained the integrity of BBB and inhibited neuronal loss following cerebral I/R challenge. Furthermore, TLB dramatically increased tight junction proteins including ZO-1, occludin and claudin 5, as well as decreased the levels of apolipoprotein E (APOE) 4, cyclophilin A (CypA), and phosphorylated nuclear factor kappa B (NF-κB), thereby reduced proinflammatory cytokines. In addition, TLB also decreased Bax/Bcl-2 ratio and cleaved-caspase 3 level along with reduced the number of apoptotic neurons. Intriguingly, molecular docking and transcriptomics predicted MMP9 was a prominent gene evoked by TLB treatment. Furthermore, the protective effect of TLB on OGD/R-induced the loss of BBB integrity in human brain microvascular endothelial cell and astrocyte co-cultures in vitro was markedly reinforced by knockdown of MMP9. Conclusions and implications: Our findings reveal a novel property of TLB: saving BBB disruption following cerebral I/R via targeting MMP9 and inhibiting APOE4/CypA/NF-κB axis.

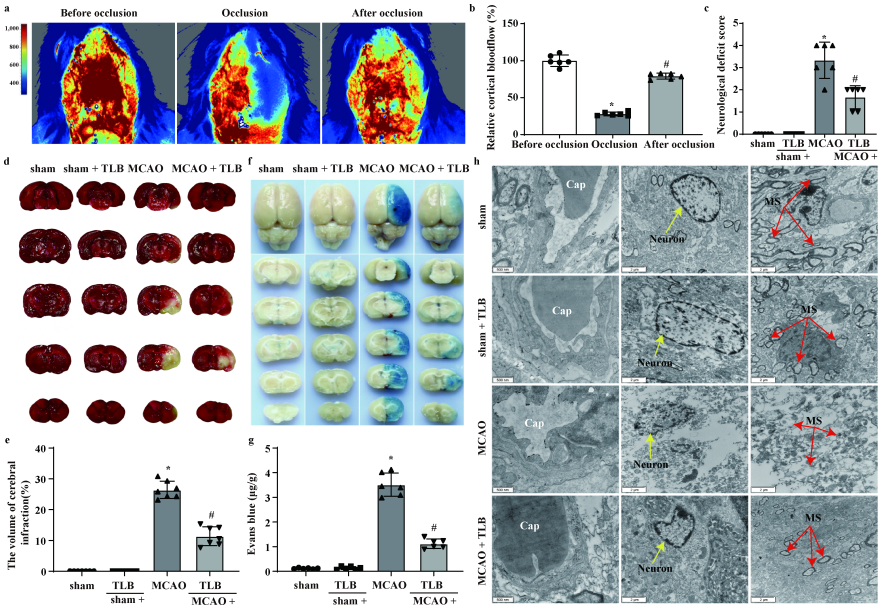

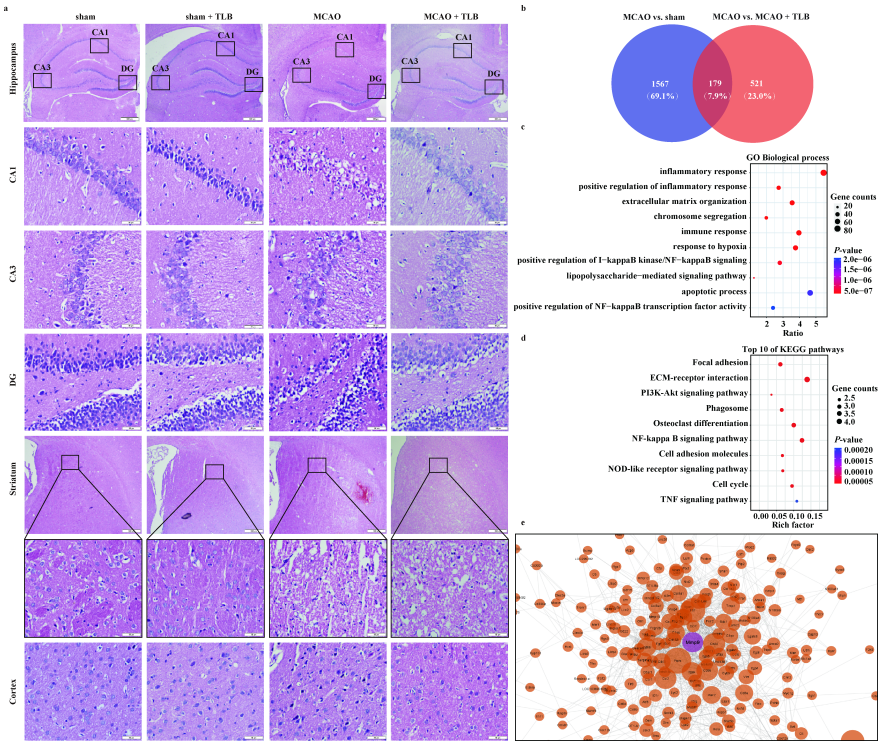

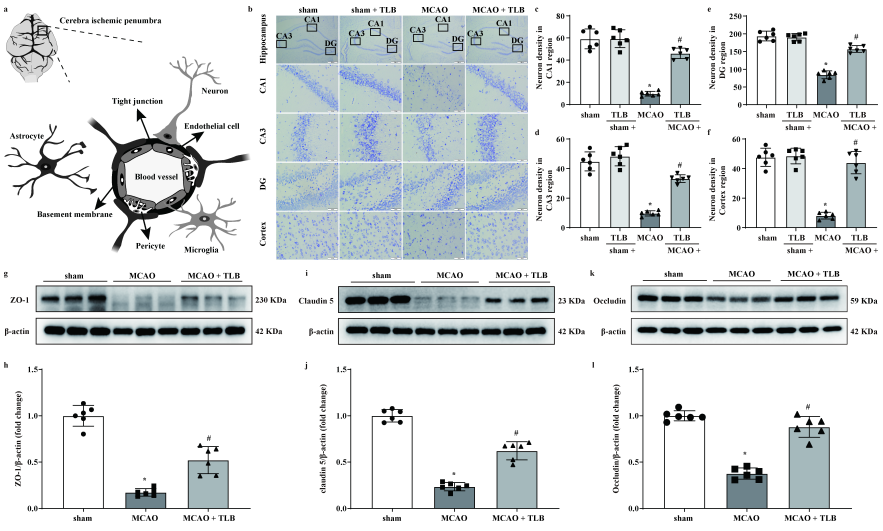

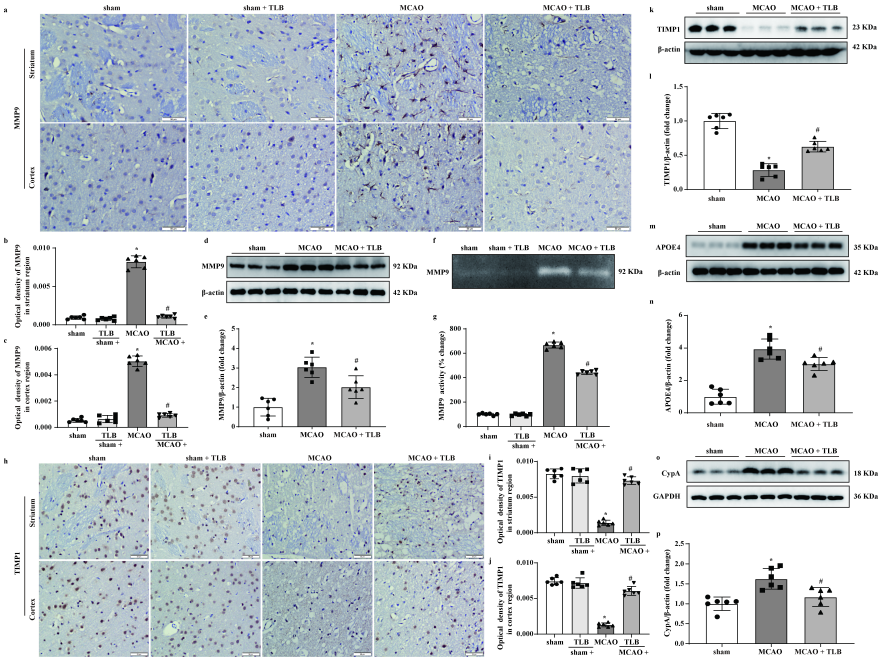

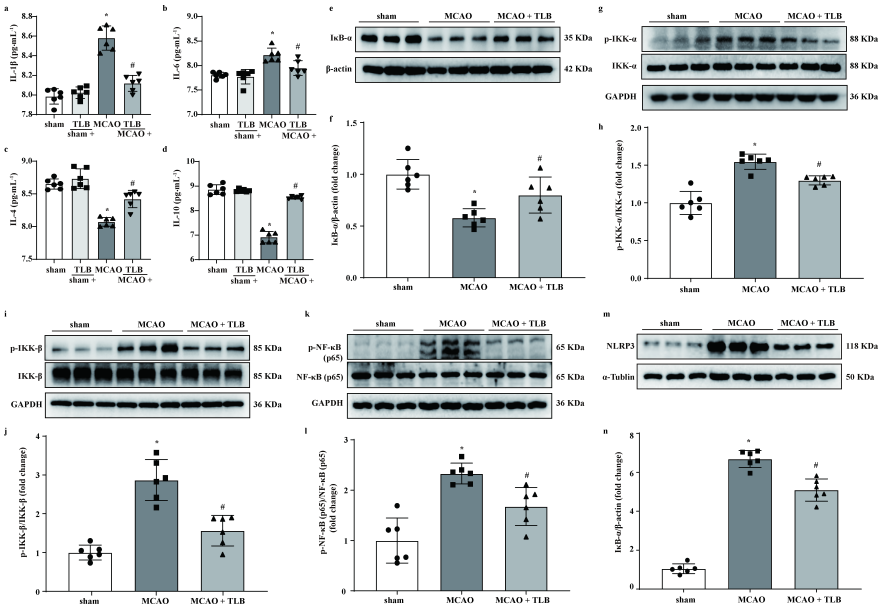

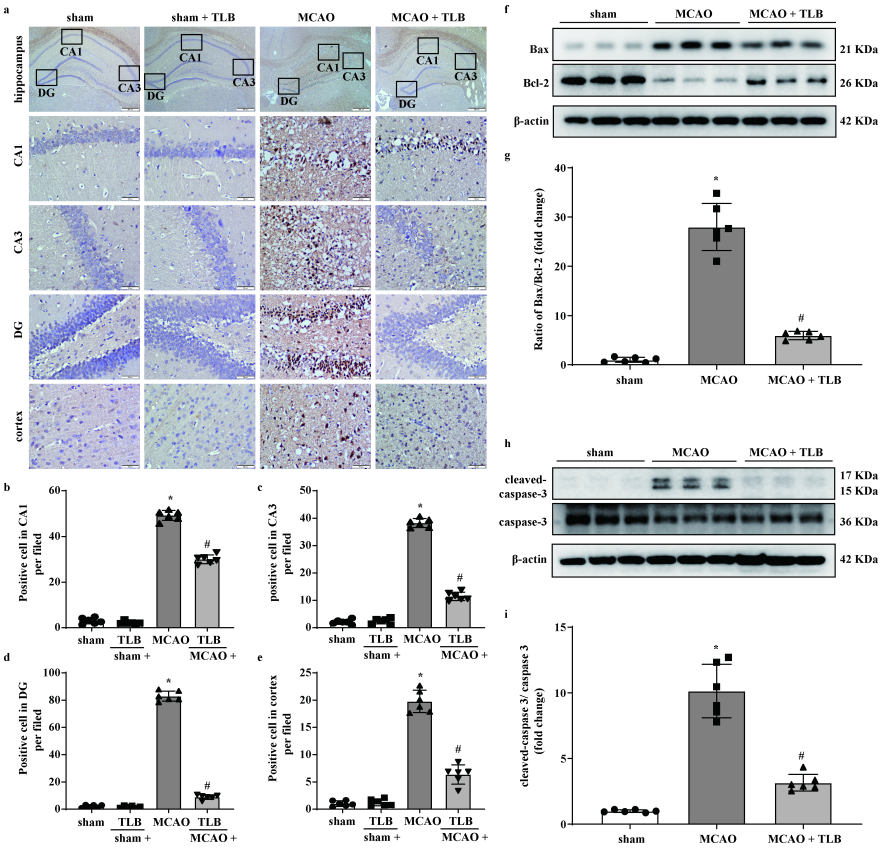

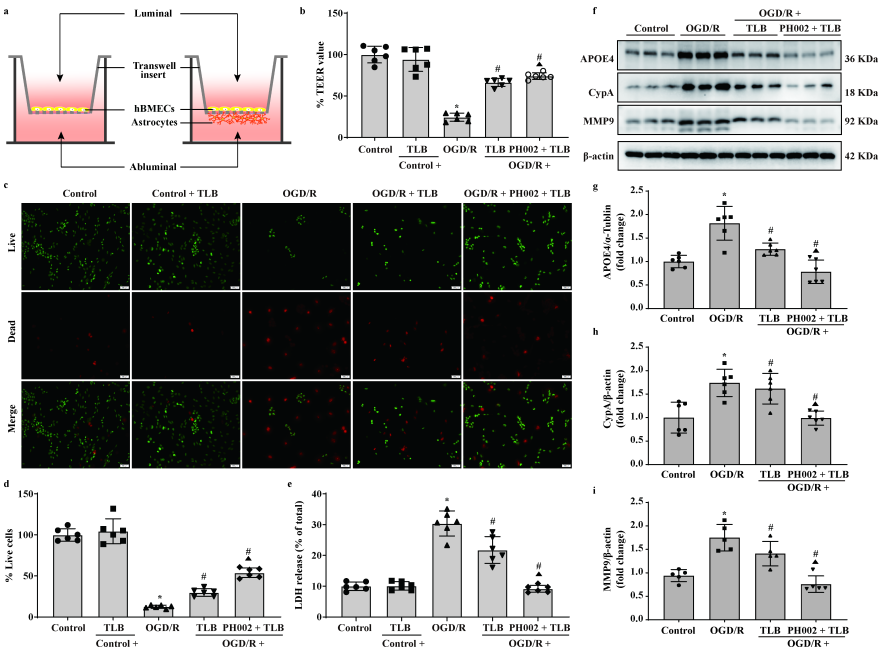

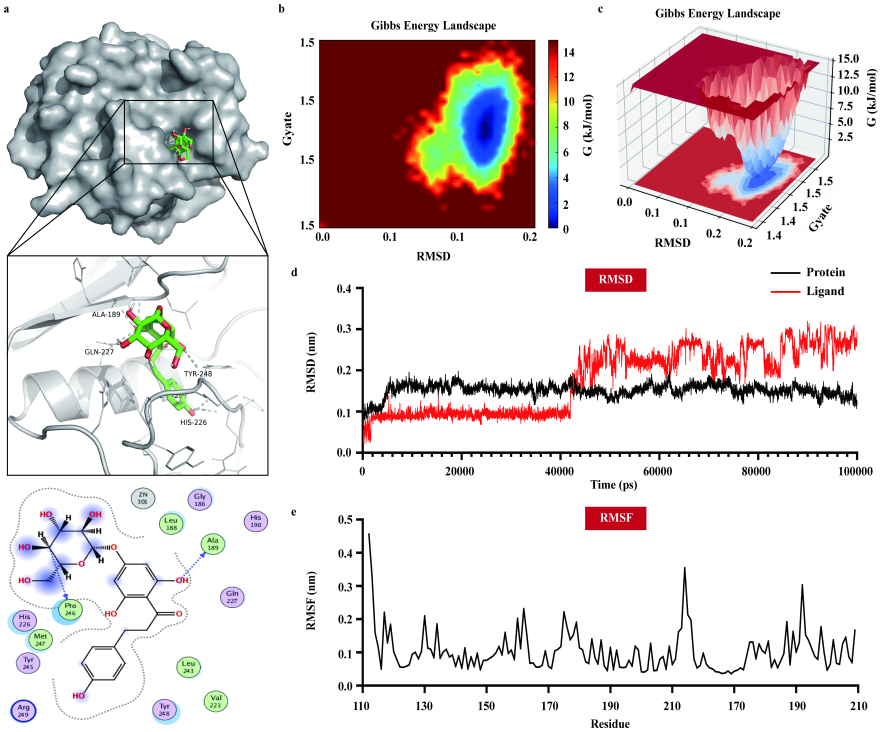

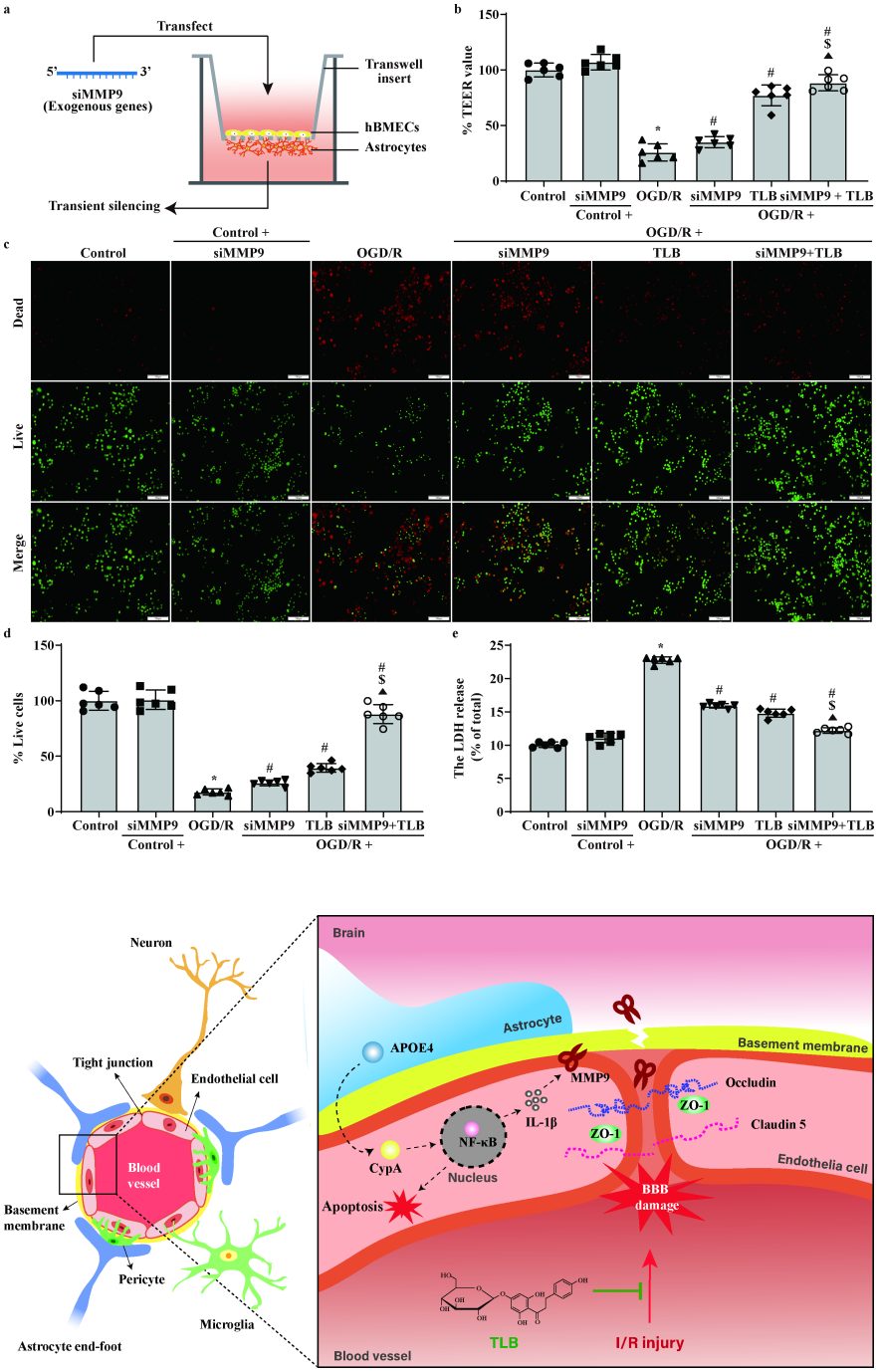

Gao Jianmei (Orcid ID: 0000-0003-3683-7956)

Trilobatin attenuates cerebral ischemia/reperfusion-induced blood-brain-barrier dysfunction by targeting MMP9: The legend of a food additive

Linying Feng[1,2], Yeli Li[1,2], Mu Lin[1,2], Dianyou Xie[1,2], Yunmei Luo[1,2], Zhixu He[3], Qihai Gong[1,2], Yizhun Zhu[1*], Jianmei Gao[1,2*]

[1]School of Pharmacy, Faculty of Medicine, Macau University of Science and Technology, Macau SAR,China

[2]Key Laboratory of Basic Pharmacology of Ministry of Education and Joint International Research Laboratory of Ethnomedicine of Ministry of Education, Zunyi Medical University, Zunyi, China

[3]The Collaborative Innovation Center of Tissue Damage Repair and Regeneration Medicine of Zunyi Medical University

These authors contributed equally to this work:

*Correspondence and requests for materials should be addressed to Jianmei Gao (gaojianmei@zmu.edu.cn) and Yizhun Zhu (yzzhu@must.edu.mo)

6 Xuefu West Road, Zunyi City, Guizhou Province, 563000, P. R. China

Tel: +86-851-286-423-03

E-mail: gaojianmei@zmu.edu.cn

Acknowledgements

This work was supported by Natural Science Foundation of China (No.82160756), Science and Technology Support Plan of Guizhou Province (No. [2020]1Y010), The hundred level of high-level innovative talents in Guizhou Province (No. QKHRCPT 20165684), Collaborative Innovation Center of Chinese Ministry of Education (No. 2020-39), Science and technology planning project of Zunyi (No. [HZ2021]187), The Natural Science Foundation of Guizhou, China (No.2019-1329).

Author contribution

LYF, YLL and ML performed the experiments. DYX and YML helped with bioinformatics analysis and molecular docking analysis. All authors were involved in analysis of data. LYF wrote the manuscript. JMG, QHG ,YZZ, and HZX design the experiments and revised the manuscript.

Confict of interest

The authors declare no conflicts of interest.

Declaration of transparency and scientific rigour

This Declaration acknowledges that this paper adheres to the principles for transparent reporting and scientific rigour of preclinical research as stated in the BJP guidelines for Design & Analysis, Immunoblotting and Immunochemistry and Animal Experimentation and as recommended by funding agencies, publishers and other organizations engaged with supporting research.

Data availability statement

The data that support the findings of this study are available from the corresponding

author upon reasonable request. Some data may not be available because of privacy or ethical restrictions.

Abstract

Background and Purpose: Blood-brain barrier (BBB) breakdown is one of the most crucial pathological changes of cerebral ischemia-reperfusion (I/R) injury. Trilobatin (TLB), a naturally occurring food additive, exerts neuroprotective effect against cerebral I/R injury as demonstrated in our previous study. This study was designed to investigate the effect of TLB on disruption of BBB after cerebral I/R injury.

Experimental Approach: Rats with focal cerebral ischemia caused by transient middle cerebral artery occlusion (MCAO) and brain microvascular endothelial cells along with human astrocytes to mimic blood brain barrier (BBB) injury caused by oxygen and glucose deprivation (OGD) followed by reoxygenation (OGD/R).

Key results: The results showed that TLB effectively maintained the integrity of BBB and inhibited neuronal loss following cerebral I/R challenge. Furthermore, TLB dramatically increased tight junction proteins including ZO-1, occludin and claudin 5, as well as decreased the levels of apolipoprotein E (APOE) 4, cyclophilin A (CypA), and phosphorylated nuclear factor kappa B (NF-κB), thereby reduced proinflammatory cytokines. In addition, TLB also decreased Bax/Bcl-2 ratio and cleaved-caspase 3 level along with reduced the number of apoptotic neurons. Intriguingly, molecular docking and transcriptomics predicted MMP9 was a prominent gene evoked by TLB treatment. Furthermore, the protective effect of TLB on OGD/R-induced the loss of BBB integrity in human brain microvascular

endothelial cell and astrocyte co-cultures *in vitro* was markedly reinforced by knockdown of MMP9.

Conclusions and implications: Our findings reveal a novel property of TLB: saving BBB disruption following cerebral I/R *via* targeting MMP9 and inhibiting APOE4/CypA/NF-κB axis.

Keywords: apolipoprotein E 4; blood brain barrier; cerebral ischemia/reperfusion; matrix metalloproteinase; trilobatin; tight junction

Abbreviations

APOE, apolipoprotein E; BBB, blood-brain barrier; BMVECs, brain microvascular endothelial cells; Cap, capillaries; CypA, cyclophilin A; DGEs, differential genes; EB, evans blue; ECM, extracellular matrix; ELISA, enzyme linked immunosorbent assay kits; ECs, endothelial cells; GO, gene ontology; HE, hematoxylin and eosin; I/R, ischemia-reperfusion; IL-1β, interleukin-1β; IHC, immunohistochemistry; KEGG, kyoto encyclopedia of genes and genomes; LDH, lactate dehydrogenase; MCA, middle cerebral artery; MCAO, middle cerebral artery occlusion; MS, myelin sheath; MMP9, matrix metalloproteinase 9; NF-κB, nuclear factor kappa B; OGD/R, oxygen glucose deprivation and reoxygenation; PPI, protein–protein interaction; rCBF, regional cerebral blood flow; root mean square deviation, RMSD; root mean square fluctuation, RMSF; SD, sprague–dawley; TTC, 2,3,5-triphenyltetrazolium chloride; TEER, transepithelial electrical resistance; TEM, transmission electron microscope; TJs, tight junctions; TNF-α, tumor necrosis factor-α; TLB, trilobatin; ZO-1, zonula occludens-1.

Bullet point summary

What is already known

• TLB, a naturally occurring food additive, possesses anti-inflammatory and anti-oxidant effects.

• TLB exerts neuroprotective effect against cerebral I/R injury.

What this study adds

• TLB confers robust protection aginst BBB disruption after cerebral I/R injury by targeting MMP9.

• APOE4/CypA/NF-κB axis is involves in the beneficial effect of TLB on BBB integrity after cerebral I/R injury.

What is the clinical significance

• TLB may be a powerful weapon in conquering ischemic stroke and expands the probability of new tactics to accomplish neuroprotection.

1. Introduction

Ischemic stroke is a debilitating neurological disorder of morbidity, mortality and ponderous socio-economic burden elicited by the break of cerebral blood flow (Ren et al., 2022). Notwithstanding the prominence as a principal cause of disability and death, efficacious treatments currently are still limited to overcome cerebral ischemic stroke. Mechanical thrombectomy and tissue plasminogen activator are the only therapeutic approaches in clinic due to both are efficient at removing the thrombus and restoring perfusion (Fischer et al., 2022). Whereas, restoration of the blood supply conquers the cerebral ischemia injury, but the damage region increasingly enlarges after the blood supply that is known as cerebral ischemia-reperfusion (I/R) injury (X.

112 Chen, Zhang, & Wang, 2022). Cerebral I/R following ischemia evokes a series of
113 events including inflammation and protease activation, all of which injure blood-brain
114 barrier (BBB) (Gong et al., 2021). The BBB comprises endothelial cells (ECs), tight
115 junctions (TJs), astrocytic end-feet processes, pericytes and the basilar membrane.
116 ECs are connected by cellular junctions, configurating a monolayer membrane of the
117 lumen in an integrated BBB (Mora et al., 2020). These cellular structures via integrins
118 to bind with the extracellular matrix (ECM), contributing to the physical barrier of the
119 BBB under steady state conditions (Calderon et al., 2022). Mechanically, the injured
120 BBB ultimately exacerbates hemorrhagic transformation and oedema, and represents
121 the mainspring of post-stroke mortality (H. Chen, Guan, Chen, Yang, & Shen, 2021).
122 Thus, salvation of BBB disruption is a dire need to prevent cerebral I/R injury and
123 will be a highly plausible tactic to treat ischemic stroke.
124 Brain microvascular endothelial cells (BMVECs) guarantee the tightness of BBB and
125 own multiple unique elements such as specialized TJs proteins including claudin-5,
126 occludin and zonula occludens-1(ZO-1) (Ng et al., 2022). Owing to the crucial
127 structures of BBB, BMVECs are rapidly activated after ischemia, along with TJs loss,
128 allowing the inflammatory cytokines including tumor necrosis factor (TNF)-α,
129 interleukin (IL)-1β, IL-6 into the brain and eventually leading to BBB integrity
130 damage (L. Liu et al., 2022). Emerging evidence demonstrates that apolipoprotein E
131 (APOE) 4, cyclophilin A (CypA), nuclear factor kappa B (NF-κB) and matrix
132 metalloproteinase (MMP) 9 have momentous and necessary roles in BBB disruption
133 after ischemic stroke (Montagne, Nation, & Zlokovic, 2020; Palomino-Antolin et al.,

134 2022). APOE4, an isoform of APOE, is substantially secreted by astrocytes and
135 promotes BBB susceptibility to damage (Nikolakopoulou et al., 2021). Suppression of
136 the proinflammatory CypA/NF-κB/MMP9 pathway is required for maintaining the
137 BBB integrity. Intriguingly, recent study reports that APOE4 accelerates loss of
138 pericyte and promotes activation of CypA/NF-κB/MMP9 pathway, which can
139 aggravate the BBB breakdown (Bell et al., 2012). However, whether
140 APOE4/CypA/NF-κB/MMP9 axis participates in the development of I/R is still blurry.
141 Trilobatin (TLB), a naturally occurring sweetener, is derived from leaves of
142 *Lithocarpus polystachyus Rehd*., which is used as a folk medicine, and has been
143 accepted as a new food material in China since 2017 (Shang et al., 2022). Amounting
144 evidence reports that TLB possesses pleiotropic pharmacological effects including
145 anti-inflammatory, anti-oxidative and anti-fatigue activities, etc (Fan et al., 2015; J.
146 Gao et al., 2018; Xiao et al., 2022). Interestingly, our previous studies have
147 discovered that TLB exerts excellent neuroprotective effects with an excellent safety
148 profile and BBB permeability (N. Chen et al., 2020; J. M. Gao et al., 2022). Recently,
149 we have found that TLB significantly reduces infarct size and restores neurological
150 functions after middle cerebral artery occlusion (MCAO) insult *in vivo*; and also
151 inhibits oxygen glucose deprivation (OGD) followed by reoxygenation (OGD/R)-
152 induced neuronal damage due to its anti-neuroinflammatory and anti-antioxidative
153 properties (J. Gao, Chen, et al., 2020). However, whether TLB can confer BBB
154 protection, and its potential mechanism associated with APOE4/CypA/NF-κB/MMP9
155 axis is still ill-defined.

156 Hence, the present study was designed to explore whether TLB evokes BBB
157 neuroprotection in MCAO-induced cerebral I/R injury in rats, and oxygen and
158 OGD/R-induced injury in co-cultured human BMVECs and astrocytes *in vitro via*
159 modulating the APOE4/CypA/NF-κB/MMP9 axis.

160 **2. Materials and methods**

161 ***2.1 Animals***

162 The male sprague–dawley (SD) rats (250–280 g) were supported by Hunan SJA
163 Laboratory Animal Co., Ltd (Changsha, China; Certificate No. SCXK2019-0004). All
164 rats were housed in specific pathogen-free facility with controllable room temperature
165 of 25 ± 1°C and a relative humidity of 55% ± 5% with 12:12 h light/dark cycle, fed on
166 a laboratory standard diet and received tap water freely. Animals were randomly
167 assigned to different experimental groups, and data was analyzed by a blinded
168 investigator. All animal experiments were approved by the Ethics Committee of Zunyi
169 Medical University (Guizhou, China, No. ZMU21-2203-583) and all the experimental
170 processes were performed according to the US National Institutes of Health guide for
171 the care and use of Laboratory animals (National Institutes of Health Publication 85-
172 23, revised 1996). Animal studies are reported in compliance with the ARRIVE
173 guidelines(Kilkenny et al., 2010; McGrath, Drummond, McLachlan, Kilkenny, &
174 Wainwright, 2010).

175 ***2.2 Induction of focal cerebral ischemia and drug delivery***

176 The male SD rats underwent right middle cerebral artery (MCA) occlusion (MCAO)
177 was used as an experimental model of cerebral I/R injury as described in our previous

178 study (J. Gao, Long, et al., 2020). In brief, rats were anesthetized with 1.5% isoflurane
179 and then isolated the external carotid artery, right common carotid artery, and internal
180 carotid artery carefully. A monofilament nylon suture with a spherical diameter of
181 0.36 mm was inserted through the external carotid artery into internal carotid artery to
182 block blood flow to the MCA (Cat#2636A4, Cinnontech Co., Ltd, Beijing, China).
183 Thereafter, then monofilament nylon suture was withdrawn after 2 h to allow
184 reperfusion for 3 days, and the rat body temperature was kept at 37 °C during surgery.
185 The perfusion and oxygenation imager (Moor Instruments, Ltd., Millwey, Axminster,
186 UK) was used to monitor the cortical blood flow as reported previously. After
187 excluding the false-positive results in the MCAO group, the survival rate of the rats
188 under anesthesia was more than 80%. Moreover, rats with convulsions, sustained
189 impaired consciousness, or no apparent dysfunction of the contralateral limb were
190 excluded from the follow-up study.

191 Following the surgical procedure, the rats were intragastric administration by TLB
192 (purity ≥98%, Cat#4192-90-9, Shanghai Renjie Biotechnology Co., Ltd, Shanghai,
193 China) at different dose of 5, 10, 20 $mg \cdot kg^{-1} \cdot d^{-1}$. The total number of SD rats were 80,
194 and the rats were randomly allocated into four groups (n = 20 per group): sham group,
195 sham + TLB (20 $mg \cdot kg^{-1} \cdot d^{-1}$) group, MCAO group, MCAO + TLB (20 $mg \cdot kg^{-1} \cdot d^{-1}$)
196 group. The rats in sham group and sham + TLB (20 $mg \cdot kg^{-1} \cdot d^{-1}$) group received the
197 same surgical procedure except for inserting the monofilament. Rats in sham + TLB
198 and MCAO + TLB groups were given TLB at doses of 20 $mg \cdot kg^{-1}$, twice a day by
199 gavage after surgery for 3 days. Meanwhile, rats in the sham and MCAO groups were

given volume-matched saline.

2.3 Cerebral blood measurement (CBF)

The CBF was detected by the moorO^2 Flo imager (Moor Instruments, Ltd., Millwey, Axminster, UK). Briefly, the rats were anesthetized till unconsciously and placed under the moorO^2 Flo imager at a distance of 20-30 cm. The midline scalp incision was made to expose the skull intact and proceed at 20 frames per second for 2 minutes. Rats were imaged pre-MCAO, post-MCAO and post-reperfusion. The region of interest (ROI) located in the main MCA area was identified and applied for analysis. The flux values were measured at each time point for each ROI of the ipsilateral and contralateral hemispheres, and ipsilateral fluxes were expressed as % of contralateral fluxes. The analysis was carried out under blind conditions.

2.4 Neurological deficit scoring and infarct volume assessment

The neurological deficits after MCAO insult were monitored by the 5-point scoring method as described previously (J. Gao, Chen, et al., 2020). After neurological function test, rats were anesthetized with1.5% isoflurane and sacrificed under anesthesia. The 2,3,5-triphenyl tetrazolium chloride (TTC, Sigma-Aldrich, St. Louis, MO, USA) staining was used to determine infarct volume as described in our previous study (J. Gao, Long, et al., 2020).

2.5 Evans blue (EB) staining

The permeability of the BBB was evaluated by the leakage of evans blue (EB, Cat#314-13-6, Sigma-Aldrich, St. Louis, MO, USA) dye into the brain through the tail vein injection as descripbed previously (Kim et al., 2020). In brief, the 2% EB (4

222 mL·kg^{-1}) was injected intravenously *via* the tail vein and allowed to circulate for 2 h.
223 Then animals were anesthetized and perfused with 0.1 M phosphate buffered saline
224 (PBS) (pH 7.4) through the left ventricle. Thereafter, the brain was immediately
225 removed and homogenize in trichloroacetic acid and centrifuged at 12,000 × *g* for 20
226 minutes. The supernatant was collected and quantitatively determined by enzyme-
227 labeled instrument (Multiskan GO, Thermo, USA).

228 ***2.6 Hematoxylin and eosin (HE) and Nissl staining***

229 HE and Nissl staining was used to determine the pathological change and neuron loss,
230 respectively, as reports previously (M. B. Liu et al., 2020). In brief, after perfused
231 with 0.1 M PBS (pH 7.4), the rat brain tissues were rapidly fixed with 4% formalin at
232 4 °C for 48 h. Thereafter, the brain sections (thickness of 3.5 μm) were dehydrated
233 and embedded in paraffin. These sections were stained with HE and Nissl at room
234 temperature, then treatment with 1% toluidine blue at 60 °C for 15 min. The changes
235 of histopathology were observed with an optical microscope (Olympus BX43, Tokyo,
236 Japan) and analyzed by Image Pro Plus 6.0 software.

237 ***2.7 Observation of transmission electron microscope (TEM)***

238 Ultrastructural change after cerebral I/R injury were observed by TEM. Briefly, brain
239 tissues were fixed in paraformaldehyde (2%) and glutaraldehyde (1%) for 8 h, and
240 then the samples were washed with 0.1 M PBS (pH 7.4). Thereafter, the samples were
241 fixed with osmium tetraoxide (1.5%) for another 2 h, and then were dehydrated and
242 embedded in araldite. Following, the brain samples were sectioned (80 nm) and
243 counterstained with uranyl acetate and lead citrate, then the capillaries (Cap), myelin

244 sheath (MS) and neurons were observed using a TEM (JEM-1400Flash, JEOL, Tokyo,
245 Japan).

246 ***2.8 Immunohistochemistry (IHC)***

247 Immunohistochemical staining was used to quantify the MMP9 and TIMP1 as
248 described previously (M. B. Liu et al., 2020). Briefly, the brains were perfused with
249 0.1 M PBS (pH 7.4) followed by 4% paraformaldehyde (Cat#P1110, Solarbio,
250 Beijing, China), dehydrated and embedded in paraffin. The brains were fixed with 4%
251 paraformaldehyde, and then was treated with dehydration and paraffin-embedded,
252 Thereafter, the 3.5-μm thick slices were prepared to be soaked in xylene and ethanol
253 to dehydration. Then, the slices were maintained with 3% aqueous hydrogen peroxide
254 for 17 min at room temperature. Following blocked with goat serum for 30 min, the
255 slices were incubated with the primary antibodies against TIMP1 (1:300,
256 Cat#ab61224, Abcam) and MMP9 (1:500, Cat#ab38898, Abcam) overnight at 4 °C,
257 and then subjected to secondary goat anti-rabbit IgG (1:500, Cat#SA00004-2,
258 Proteintech) followed by incubated with HRP-labeled streptozotocin for 20 min at
259 37 °C. After the positive cells were visualized by DAB kit (Cat#ZLI-9018, ZSGB-BIO,
260 Beijing, China), images were digitally captured by a light microscopy (Olympus BX43,
261 Tokyo, Japan) and Image Pro Plus 6.0 software for statistical analysis.

262 ***2.9 TUNEL staining***

263 The apoptosis was detected using In situ cell death detection kit, POD
264 (Cat#11684817910, Roche, Applied Science, Germany) according to the
265 manufacture's protocols (M. B. Liu et al., 2020). In brief, the paraffin embedded brain

266 tissue sections were deparaffinized with xylene and then rehydrated with graded
267 ethanol. Following, the sections were subjected to 3% H_2O_2 for 20 min and incubated
268 with proteinase K (Cat#P1120, Solarbio, Beijing, China) for 15 min at 37 °C, then
269 TUNEL staining was performed according to the manufacturer's protocol. Finally, the
270 sections were visualized with a DAB kit and the TUNEL-positive cells were observed
271 using a light microscopy (Olympus BX43, Tokyo, Japan) and Image Pro Plus 6.0
272 software for statistical analysis.

273 ***2.10 Transcriptome analysis***

274 The total RNA was extracted from the cerebral tissue of rats in sham, sham + TLB 20
275 $mg \cdot kg^{-1}$, MCAO, MCAO + TLB 20 $mg \cdot kg^{-1}$ groups by TRIzol reagent following the
276 manufacturer's protocol, and quantified by Bioanalyzer 2100 and RNA 6000 Nano
277 LabChip Kit (Agilent, CA, USA, 5067-1511) analysis meter. The qualified RNA
278 transcriptome was performed with an Illumina Novaseq™ 6000 (LC-Bio Technology
279 CO., Ltd., Hangzhou, China) following the vendor's recommended protocol. String
280 database (version 10.5) was adopted to protein interaction information, then protein–
281 protein interaction (PPI) network was constructed by Cytoscape 3.6.0 software. The
282 differential genes (DGEs) with $|\log^2 FC| > 1$ and adjusted $p < 0.05$ were considered to
283 be significantly different expressed genes. In order to intuitively observe the
284 distribution of potential DEGs, the venn diagram was performed by Venny 2.1.0[3]. In
285 addition, the gene ontology (GO) function and Kyoto Encyclopedia of Genes and
286 Genomes (KEGG) pathway enrichment analysis were performed on the up-regulated
287 DEGs using DAVID (version 6.8) software.

288 ***2.11 Enzyme linked immunosorbent assay (ELISA)***

289 The levels of inflammatory cytokines were detected by ELISA kits which purchased
290 from Shanghai Renjie Biotechnology. Briefly, the brain tissues were collected and
291 homogenized in 0.01 M ice-cold PBS (pH 7.4) and centrifuged at 3000 × *g* for 15 min
292 at 4 °C. The levels interleukin-1 β (IL-1β, Cat#RJ16944, RenjieBio), IL-6
293 (Cat#RJ16958, RenjieBio), IL-4 (Cat#RJ16956, RenjieBio) and IL-10 (Cat#RJ16932,
294 RenjieBio) were detected by ELISA kits according to the product instruction.

295 ***2.12 Gelatin zymography***

296 The activity of MMP9 in ischemic penumbra was detected by gelatin zymography
297 (Cat#P1700, Applygen, Beijing, China). Briefly, 30 μg protein samples were loaded on
298 10% triglycine gel with 0.1% gelatin as substrate for separation. After electrophoresis,
299 the gels were washed with distilled water and incubated at 37 °C for 24 h.
300 Subsequently, the gels were stained with coomassie brilliant blue staining solution
301 (Cat#P1305, Solarbio, Beijing, China) and the gels were scanned according to
302 manufacturer's instruction.

303 ***2.13 BBB model in vitro and determination of permeability***

304 BBB model *in vitro* was used to detect permeability as described previously (T. Yang
305 et al., 2018). In brief, human BMVECs (hBMECs/D3) and human astrocytes
306 (U118MG) (secondary generation cells, ATCC, Manassas, VA, USA) were cultured in
307 Dulbecco's Modified Eagle's Medium (DMEM) supplemented with fetal bovine
308 serum, 100 $U \cdot mL^{-1}$ penicillin and 100 $U \cdot mL^{-1}$ streptomycin at 37 °C under a
309 humidified atmosphere containing 5% CO_2. Transwell inserts (0.4 μm pore size) were

310 placed into 6-well plates to divide each well into luminal (top) and abluminal (bottom)
311 compartments. For the model of co-culture, human BMECs were seeded onto the
312 inserts and incubated till confluence was finished. Then inserts were reversed, and
313 astrocytes were seeded onto the reversed surface in the incubator for 20 min. After
314 BBB model achieved, hBMECs/U118MG cells were exposed to OGD/R as previously
315 described with modification. Briefly, hBMECs/U118MG co-cultures with appropriate
316 confluence washed three times with 0.01 M ice-cold PBS (pH 7.4) and the standard
317 culture medium was replaced with glucose-free earle's balanced salt solution medium.
318 Thereafter, the cells were transferred to a modular incubator chamber (MIC-101)
319 (Embrient Inc., USA) under oxygen-free N2/CO_2 (95%/5%) gas and incubated for 4 h
320 at 37 °C. The hBMECs/U118MG co-cultures of control group were cultured in
321 standard medium. Thereafter, the culture medium of OGD/R group was replaced with
322 standard medium, or treated with (6.25, 12.5, 25, 50 μM) for another 24 h.
323 Transepithelial electrical resistance (TEER) is a widely accepted quantitative
324 technique to measure the integrity of TJs in vitro BBB model. Following, TEER was
325 measured by an Millicell-ERS equipment (EMD Millipore corporation, USA), and
326 TEER values were calculated as $\Omega \cdot cm^2$ by multiplying the surface area of the
327 transwell insert as previously report.

328 ***2.14 Measurement of cell viability and death***

329 The hBMECs/U118MG co-cultures were treated as mentioned above. The cell
330 viability was detected using Live/Dead cell viability assay (Cat#501-100, Biovision,
331 USA) as previously described. In brief, hBMECs/D3 and U118MG co-cultures were

332 stained with 1 mM Live-Dye (a cell-permeable green fluorescent dye) and 1 mg·mL^{-1}
333 propidium iodide (a cell-impenetrable red fluorescent dye) incubated at 37 °C for 20
334 minutes then observed and photographed under a fluorescence microscope (Olympus
335 BX53, Tokyo, Japan). Green fluorescence represents live cells and red fluorescence
336 represents dead cells, and the percentage of dead cell (%) was calculated by the
337 percent of dead cells (red)/total cells (green and red) to represent live cells and dead
338 cells, respectively. In parallel, release of extracellular lactate dehydrogenase (LDH)
339 from injured cells was detected using LDH detection kit (Cat#RJ13762, Shanghai
340 Renjie Biotechnology Co., Ltd, Shanghai, China) according to the manufacturer's
341 protocol, and the absorbance was measured at 490 nm.

342 ***2.15 Transfection of siRNA***

343 The hBMECs/U118MG cells were transfected with 100 nM MMP9-targeted siRNA
344 (5'-GTACCGCTATGGTTACACT-3') (Cat#stB0002323A, RIBOBIO CO., LTD.
345 Guangzhou, China) or scrambled siRNA by Lipofectamine 2000 in accordance with
346 the manufacturing instructions. The knockdown of endogenous MMP9 siRNA was
347 confirmed by western blot. The transfected hBMECs/U118MG cells were subjected to
348 OGD/R after being transfected for 48 h and treated with TLB (50 μM) or PH002 (200
349 nM) (Cat#HY-112798, Medchemexpress, China) an APOE4 inhibitor. Thereafter,
350 Live/Dead cell viability, LDH release, protein expressions of APOE4, CypA, and
351 MMP9 were determined in the following experiments.

352 ***2.16 Western blot***

353 The protein samples from the ischemic penumbra were dissolved in RIPA buffer

354 (Cat#R0010, Solarbio, Beijing, China) which contained proteinase inhibitor PMSF
355 (Cat#P0100, Solarbio, Beijing, China). The lysate was centrifuged at 15,000 × *g* for 15
356 min at 4 °C. Then the protein concentration was determined by BCA protein assay kit
357 (Cat#PC0020, Solarbio, Beijing, China). Subsequently, a 30 μg aliquot of the protein
358 samples from each group were loaded onto a 6-12% sodium dodecyl sulfate–
359 polyacrylamide gel electrophoresis and electro-transferred to a nitrocellulose
360 membrane. Thereafter, the membranes were blocked in 5% (w/v) non-fat powdered
361 milk (Cat#A600669-0250, Solarbio, Beijing, China) for 2 h at room temperature, then
362 incubated with primary antibodies against MMP9 (1:1000, Cat#38898, Abcam),
363 TIMP1 (1:2000, Cat#61224, Abcam), claudin 5 (1:2000, Cat#5216, Affinity
364 Biosciences), occludin (1:5000, Cat#167161, Abcam), ZO-1 (1:1000, Cat#21773-1-
365 AP, Proteintech), APOE4 (1:1000, Cat#279714, Abcam), CypA (1:1000, Cat#41684,
366 Abcam), NF-κB p65 (1:1000, Cat#16502, Abcam), phosphorylation-NF-κB (1:1000,
367 Cat#82699, Abcam), IκB-α (1:1000, Cat#32518, Abcam), phosphorylation-IKK-α
368 (1:1000, Cat#38515, Abcam), IKK-α (1:1000, Cat#38575, Abcam), phosphorylation-
369 IKK-β (1:1000, Cat#194519, Abcam), IKK-β (1:1000, Cat#124975, Abcam), NLRP3
370 (1:1000, Abcam, Cat#263899), caspase 3 (1:1000, Cat#13847, Abcam), cleaved-
371 caspase 3 (1:2000, Cat#2302, Abcam), Bcl-2 (1:1000, Cat#59348, Abcam), Bax
372 (1:1000, Cat#32503, Abcam), GAPDH (1:2000, Cat#60004-1-lg, Proteintech), α-
373 Tublin (1:2000, Cat#11224-1-AP Proteintech), and β-actin (1:2000, Cat#66009-1-lg,
374 Proteintech) overnight at 4 °C. Subsequently, the bands were incubated with
375 secondary antibody HRP-conjugated Affinipure Goat Anti-Mouse IgG (H+L) (1:5000,

376 Cat#SA00001-1, Proteintech) or HRP-conjugated Affinipure Goat Anti-Rabbit IgG
377 (H+L) (1:5000, Cat#SA00001-2, Proteintech) for 2 h at room temperature. Then,
378 representative bands were visualized with ECL detection reagents (Cat#MA0186,
379 Meilunbio, Shanghai, China) and quantified on a ChemiDoc MP Imaging System
380 (Bio-Rad Laboratories, Inc., Hercules, CA, USA).

381 ***2.17 Molecular docking***

382 The affinity between TLB and APOE4, CypA, NF-κB or MMP9 were predicted using
383 in silico computational molecular docking as described in our previous study(Zheng
384 et al., 2020). In brief, the three-dimensional protein structures of APOE4 (PDB ID:
385 1GS9), CypA (PDB ID: 1L6J), NF-κB (PDB ID: 1MY5) and MMP9 (PDB ID: 1L6J)
386 were retrieved from the protein data bank (PDB). The autodock 4.2 software and
387 PyMOL software were used to determine the interaction of TLB and APOE4, CyA,
388 NF-κB or MMP9.

389 ***2.18 Molecular Dynamic (MD) simulation***

390 Gromacs2022.3 software was used for molecular dynamics simulation. For small
391 molecule preprocessing, AmberTools22 is used to add GAFF force field to small
392 molecules, while Gaussian 16W is used to hydrogenate small molecules and calculate
393 RESP potential. Potential data will be added to the topology file of molecular
394 dynamics system(Abraham, Murtola, Schulz, Páll, & Lindahl, 2015; Van Der Spoel et
395 al., 2005). The simulation system adopts the steepest descent method to minimize the
396 energy, and then carries out the isothermal isovolumic ensemble (NVT) equilibrium
397 and isothermal isobaric ensemble (NPT) equilibrium for 100000 steps, respectively,

398 with the coupling constant of 0.1 ps and the duration of 100ps. Finally, the free
399 molecular dynamics simulation was performed. The process consisted of 5000000
400 steps, the step length was 2fs, and the total duration was 100ns. After the simulation
401 was completed, the built-in tool of the software was used to analyze the trajectory, and
402 the root-mean-square variance (RMSD), root-mean-square fluctuation (RMSF) and
403 protein rotation radius of each amino acid trajectory were calculated, combined with
404 the free energy (MMPBSA), free energy topography and other data.

405 ***2.19 Statistical analysis***

406 The data and statistical analysis were in line with the *British Journal of*
407 *Pharmacology* guidelines on experimental design and analysis (Curtis, Ashton, Moon,
408 & Ahluwalia, 2018). All values were expressed as mean ± SD and analyzed using
409 GraphPad Prism 5.0 software (GraphPad Software, San Diego, CA, USA), where n
410 represents the number of independent experiments and not replicates. All experiments
411 were designed to generate groups of equal size, using randomization and blinded
412 analysis. All the statistical analysis were performed only for studies containing at least
413 5 independent values ($n \geq 5$), and no values were excluded from the data used for
414 statistical analysis. Statistical significance between two independent groups was
415 analyzed using unpaired two-tailed Student's t test or multiple comparison were
416 performed using one-way analysis of variance (ANOVA) followed by Bonferroni's
417 *post hoc* test. $P < 0.05$ was considered a statistically significant difference.

418 **3. Results**

419 ***3.1 TLB effectively protects against BBB disruption after cerebral I/R insult***

420 The rats underwent MCAO/R to achieve cerebral I/R animal model as described in
421 our previous study. First, the regional cerebral blood flow (rCBF) decreased to less
422 than 20% and recovered to more than 80% of baseline, indicating that a successful
423 cerebral I/R model was achieved (Fig.1a, b). Subsequently, the results showed that
424 TLB significantly reduced the neurological deficits and cerebral infract volume after
425 cerebral I/R injury in rats (Fig.1c-e), in consistent with our previous findings. Based
426 on these results, BBB integrity and ultrastructural changes were observed by EB
427 leakage staining and TEM. The results showed that leakage of EB dye was
428 significantly increased in MCAO group in comparison with sham group, suggesting
429 that cerebral I/R injured BBB integrity. Whereas, TLB markedly decreased the
430 leakage of EB dye after cerebral I/R injury (Fig.1f, g). Furthermore,
431 the cap appeared stenosis, the neuron morphology became atypically disorganized and
432 MS was unclear or with demyelination in comparison with sham group. However,
433 TLB reversed these ultrastructural changes (Fig. 1h). These findings demonstrate that
434 the BBB protection is involved in the neuroprotective effect of TLB against cerebral
435 I/R injury.

436 ***3.2 TLB suppresses injury to the hippocampus, cortex and striatum following***
437 ***cerebral I/R injury and microarray data analysis***

438 HE staining was applied to determine the effects of TLB on histopathological changes
439 after cerebral I/R injury. The results showed that cell boundary and the numbers of
440 neurons in hippocampus (CA1, CA3, DG regions), cortex and striatum disappeared or
441 reduced after cerebral I/R insult. However, TLB significantly reversed these changes

442 in hippocampus (CA1, CA3, DG regions), cortex and striatum (Fig. 2a). These
443 findings indicate that TLB effectively suppresses cerebral I/R-induced neuronal
444 damage in hippocampus, cortex and striatum. To investigate the potential molecular
445 mechanisms of TLB effects in I/R rats, we detected the transcriptome of cerebral
446 tissue in rats. We discovered that up-regulation of 1567 DEGs were analyzed in
447 MCAO versus sham group, while 521 DEGs were analyzed in MCAO versus MCAO
448 + TLB group. In addition, 179 of 700 DEGs that responded to TLB treatment were
449 related with DEGs caused by brain I/R injury, according to a Venn diagram (Fig. 2b).
450 Moreover, GO terms enrichment and KEGG pathways were described for the selected
451 1764 DEGs. As the results, GO enrichment analysis showed that DEGs involved in
452 inflammation response, hypoxia, positive regulation of IκB-α kinase/NF-κB signaling,
453 positive regulation of NF-κB transcription factor activity, and apoptotic process, et al.
454 (Fig. 2c). In addition, KEGG enrichment analysis showed that DEGs participated in
455 many signaling pathways, such as focal adhesion, PI3K-Akt signaling pathway, cell
456 adhesion molecules, NF-κB signaling pathway, NOD-like receptor signaling pathway,
457 and TNF signaling pathway (Fig. 2d). Furthermore, a total of 700 DEGs were
458 identified after TLB treatment that analyzed by PPI. These DEGs encode 2884 pairs
459 of interacting proteins, and the size of the circle represents the degree to which the
460 protein is associated with other proteins. Obviously, MMP9 was involved in 336
461 interactions, suggesting that MMP9 may be the main relevant signaling molecule (Fig.
462 2e).

463 ***3.3 TLB suppresses loss of neuron and TJ proteins after cerebral I/R insult***

464 BBB breakdown after stimulation of cerebral I/R injury subsequently leads to
465 neuronal loss and impairment of TJs (Fig. 3a). Hence, we determined whether TLB
466 affects the neurons and the expression of TJ proteins. The results showed that the
467 Nissl body dissolution in hippocampus (CA1, CA3, DG regions) and cortex were
468 decreased in MCAO group than those of sham group as evidenced by Nissl staining.
469 Whereas, TLB significantly increased the number of Nissl bodies (Fig. 3b-f).
470 Moreover, TJ proteins including ZO-1, claudin 5 and occludin protein expressions
471 were increased in MCAO group in comparison with sham group. However, TLB
472 significantly increased the expression of TJ proteins after cerebral I/R injury (Fig. 3g-
473 l). These findings demonstrate that TLB effectively maintain the BBB integrity
474 through protecting against loss of neuron and impairment of TJs.

475 ***3.4 TLB balances TIMP1/MMP9 and suppresses APOE4/CypA signaling pathway***
476 ***after cerebral I/R insult***

477 According to the results of transcriptomics, MMP9/TIMP1 balance, APOE4 and
478 CypA protein expressions, as well as MMP9 activity were measured. The results
479 showed that distribution and expression of MMP9 as well as its activity were
480 increased in MCAO group than those in sham group (Fig. 4a-g). While, distribution
481 and expression of TIMP1 were decreased in MCAO group than those in sham group
482 (Fig. 4h-l). However, TLB obviously reversed these changes in the cortex and
483 striatum after cerebral I/R injury. Furthermore, the results showed that the protein
484 expression of APOE4 (Fig. 4m, n) and CypA (Fig. 4o, p) protein expression were
485 significantly increased in MCAO group in comparison of sham group. Whereas, these

486 increases were significantly reduced by TLB. These findings suggest that
487 MMP9/TIMP1 balance and APOE4/CypA signaling are participate the protective
488 effect of TLB against BBB disruption.

489 ***3.5 TLB inhibits neuroinflammation via regulating NF-κB signaling pathway after***
490 ***cerebral I/R insult***

491 Since neuroinflammation plays a vital role in the BBB breakdown following cerebral
492 I/R injury, we thereafter determined the effect of TLB on cytokines release and NF-
493 κB signaling pathway. The results showed that the pro-inflammatory cytokines IL-1β
494 and IL-6 were increased, and the anti-inflammatory cytokines IL-4 and IL-10 were
495 decreased in MCAO group compared to sham group; Whereas, TLB significantly
496 reversed these changes after cerebral I/R injury (Fig. 5a-d). Furthermore, the protein
497 expression of IκB-α was decreased in MCAO group compared to sham group.
498 However, TLB significantly increased the protein expression of IκB-α after cerebral
499 I/R injury (Fig. 5e, f). In addition, protein phosphorylation levels of NF-κB p65, IKK-
500 α, IKK-β and the expression of NLRP3 were increased in MCAO group compared to
501 sham group. Whereas, TLB markedly reversed these changes (Fig. 5g-n). These
502 findings indicate that TLB also effectively inhibits neuroinflammation after cerebral
503 I/R insult.

504 ***3.6 TLB suppresses neuronal death through inhibiting caspase 3-dependent***
505 ***apoptosis pathway after cerebral I/R injury***

506 In addition, TUNEL staining and Western blot were used to confirm the anti-apoptotic
507 effects of TLB on neurons in cerebral I/R-induced BBB breakdown. The results

508 showed that the TUNEL-positive cells were increased in CA1, CA3, DG regions of
509 hippocampus and cortex in MCAO group compared to sham group. However, TLB
510 significantly reduced the TUNEL-positive cells in hippocampus and cortex after
511 cerebral I/R injury (Fig. 6a-e). Furthermore, Bax/Bcl-2 ratio and the protein level of
512 cleaved-caspase 3 were up-regulated in MCAO group compared to sham group.
513 Whereas, TLB markedly reversed these changes (Fig. 6f-i). These findings indicate
514 that TLB effectively hinders the BBB disruption-elicited neuronal death, at least
515 partly, through inhibiting caspase 3-dependent apoptosis pathway.

516 ***3.7 TLB inhibits loss of BBB integrity through activating APOE4/CypA/MMP9***
517 ***signaling pathway after OGD/R insult in vitro***

518 To further investigate the mechanism of TLB-evoked BBB protection after cerebral
519 I/R injury, we used human BMEC (hBMECs/D3) and astrocytes (U118MG) co-
520 cultures *in vitro* to mimic cerebral I/R-induced BBB breakdown *in vitro*. TEER value
521 is deemed as a bio-indicator of BBB integrity study *in vitro* due to it can reflect the
522 integrity of cell. The BBB model *in vitro* was accepted when the TEER value of
523 200~300 $\Omega\cdot cm^2$. The results showed that TLB (12.5, 25, 50 μM) not only
524 significantly increased TEER value, but also inhibited the cellular death after OGD/R
525 insult, as evidenced by Millicell-ERS equipment and LDH leakage, respectively
526 (Supplementary Fig. S1). Whereas, PH002, an APOE4 inhibitor, strengthened the
527 beneficial effects of TLB on OGD/R-induced cellular integrity injury (Fig. 7a-e),
528 which suggested that TLB conferred BBB protection was required APOE4.
529 Subsequently, in keeping with the results in *in vivo*, APOE4, CypA and MMP9 protein

530 expressions were increased after OGD/R insult. However, TLB significantly reversed
531 these changes (Fig. 7f, i). Interestingly, PH002 reinforced the inhibitory effects of
532 TLB on APOE4, CypA and MMP9 protein expressions upon OGD/R (Fig. 7f, i).
533 These results suggest that APOE4/CypA/MMP9 pathway is involved in TLB-evoked
534 BBB protection.

535 ***3.8 The interaction between TLB and MMP9***

536 To further clarify the potential targets of TLB as mentioned above, we used in silico
537 computational molecular docking to predict the affinity between TLB and APOE4,
538 CypA or NF-κB. The data displayed that the binding energy between TLB and
539 APOE4, CypA or MMP9 was -4.26, -4.97, or -7.2 $kcal \cdot mol^{-1}$, which indicated that
540 TLB could bind to MMP9, but not APOE4 and CypA (Fig. 8a). These results suggest
541 that TLB could directly combined with MMP9, thus activate the MMP9 signaling
542 pathway. The gibbs energy landscape helps to understand conformational change and
543 energy minimization. The dark blue is the energy minimum, means the lowest energy
544 and the dispersion represents the flexibility of the conformation. The results showed
545 that a large area was presented in the plot for TLB-MMP9 complex, suggest there is
546 no significant conformational changes in the complex structure (Fig. 8b). In the gibbs
547 energy profile, purple represents the energy minimum, the greater the energy
548 minimum is, the better the structural stability of the complex. The TLB-MMP9
549 complex depicts the stability which correlates the previous gibbs energy landscape
550 (Fig. 8c). Moreover, The RMSD of protein backbone indicates the structural stability
551 during MD simulations. As shown in Fig. 8d, The protein structure was stable during

552 100000 ps MD simulation. Different flexibility of MMP9 binding sites were observed
553 by RMSF analysis, as a result, most MMP9-bound residues exhibited less flexibility
554 with RMSF less than 0.5 Å, suggesting that these residues showed stronger rigidity
555 due to binding with TLB (Fig. 8e). These results indicate that the TLB was stably
556 targeting the MMP9.

557 ***3.9 TLB exerts protective effect on OGD/R-induced BBB integrity disruption***
558 ***through directly bind to and hinders MMP9***

559 Furthermore, knock down of MMP9 by siRNA in human BMEC/astrocytes co-
560 cultures substantially strengthened the protective effect of TLB on OGD/R-induced
561 impairment of BBB integrity (Fig. 9a). As evidenced by increase of TEER value and
562 cell viability and decrease of LDH leakage (Fig. 9b-e). These findings confirm that
563 MMP9 might be the potential therapeutic target of TLB against cerebral I/R-induced
564 BBB disruption.

565 **4. Discussion**

566 The present study unveils, for the first time, that (1) TLB confers BBB protection on
567 I/R injury due to decrease neuroinflammation and inhibit caspase-3-dependent
568 apoptosis; (2) TLB evokes robust BBB protection *via* APOE4/CypA/NF-κB signaling
569 pathway; (3) TLB interacts with MMP9, and the protective effects of TLB on BBB
570 are strengthened by knockdown of MMP9 (Fig. 10). Collectively, our findings
571 uncover a novel property of TLB: rescuing BBB breakdown after cerebral I/R injury
572 by targeting MMP9 via mediating APOE4/CypA/NF-κB pathway, and put forward
573 "proof-of-concept" for BBB protection of TLB against cerebral ischemic stroke.

574 The BBB plays the prominent role in keeping homeostasis within the central nervous
575 system through blocking foreign substances from the blood into the brain tissue
576 (Chang et al., 2017). Cerebral I/R elicits BBB endothelial cell lesion and BBB
577 destruction, which is linked with BBB leakage, incremental permeability and
578 inflammatory cell infiltration (Lama et al., 2022; Lei et al., 2021), yet there are still
579 unapproachable to efficacious clinic interventions of BBB breakdown following
580 cerebral I/R injury. Our previous study revealed that TLB effectively protected against
581 cerebral I/R injury inasmuch as it possesses excellent anti-inflammatory property (J.
582 Gao, Chen, et al., 2020). However, whether TLB can rescue the BBB disruption after
583 cerebral I/R injury is still obscure. Encouragingly, the present study corroborates and
584 extends our previous findings that TLB at the most effective dose of 20 $mg \cdot kg^{-1}$
585 reduced neurological dysfunction and cerebral infarction in MCAO/R rat model,
586 which are consistent with our previous research results. Furthermore, we found that
587 EB leakages, hippocampal and cortical neuron damage were significantly augmented
588 in the ischemic zone, indicating that cerebral I/R injury causes severe BBB
589 destruction. By comparison, TLB markedly decreased BBB permeability and
590 prevented neuronal damage, suggesting that preserving BBB integrity contributes to
591 TLB's neuroprotective effects on ischemic stroke. In addition, the breakdown of the
592 BBB after cerebral I/R produces degradation of TJs and direct or indirectly cause loss
593 or injured neurons. Encouragingly, the results showed that TLB effectively blocked
594 neuron loss in hippocampus and cerebral cortex after cerebral I/R challenge. These
595 results are also well elucidated our previous findings that TLB restores long-term

596 neurological functions upon cerebral I/R injury.

597 What's more, TJs involve a sequence of proteins distributed between endothelial cells
598 and are responsible for maintaining the BBB integrity (Ben-Zvi et al., 2014). The
599 results in this study showed that TLB dramatically increased TJs including ZO-1,
600 occludin and claudin 5 upon cerebral I/R, which suggested that TLB preserved BBB
601 integrity and rescued neuron loss through maintaining TJs. However, the detailed
602 mechanisms that mediate BBB protection of TLB is blurry. Subsequently,
603 transcriptome analysis was utilized to predict the possible underlying mechanism of
604 TLB-triggered BBB protection. Transcriptomics pointed out that DEGs were
605 primarily enriched in ECM-receptor interaction, cell adhesion molecules,
606 inflammatory response, IκB/NF-κB and apoptosis signaling pathways. Importantly,
607 there is a potent interaction between the MMP9 signaling molecule and the DEGs
608 induced by TLB. Taking clues from the transcriptomics data we thereafter quest to
609 validate these findings in the MCAO/R rat model. Cerebral I/R injury results in
610 intricate signaling pathways inducing apoptosis, a type of programmed cell death
611 (Matei et al., 2018). In damaged brain tissue, there were multiple genes that modulate
612 neuronal apoptosis, involving Bcl-2 (a gene that hinders apoptosis) and Bax (a gene
613 that accelerates apoptosis) and caspase 3(Cai et al., 2022; Yu et al., 2022). The
614 heterodimer of Bcl-2/Bax will be formed to hinder apoptosis when the expression of
615 Bcl-2 augmented. In contrast, the homodimer of Bax/Bax will be formed to accelerate
616 apoptosis when the expression of Bax augmented (Richter et al., 2022). Thus,
617 Bax/Bcl-2 ratio can reflect the tendency of cell towards to apoptosis or survival upon

618 stimuli. While, caspase 3 is a crucial modulator of apoptosis and involves in the
619 cellular death signaling transduction (Khalifa, El Sokkary, Elblehi, Diab, & Ali, 2022).
620 Our results demonstrated that Bax/Bcl-2 ratio and cleaved-caspase 3 in ischemic
621 penumbra tissues significantly increased after cerebral I/R injury, whereas these
622 increases were reversed by TLB. Of note, recent studies report that injured neurons
623 induced by neuronal apoptosis in hippocampus and cerebral cortex occurred following
624 cerebral I/R injury (Z. Yang et al., 2022). We found that TLB effectively reduced
625 numbers of apoptotic cell in hippocampus and cerebral cortex of ischemic penumbra
626 after cerebral I/R injury. Besides, NF-κB/NLRP3 axis is involved in BBB disruption
627 and induces apoptosis after cerebral I/R injury (Iorio, Celenza, & Petricca,
628 2022).NLRP3 is a prominent modulator of neuroinflammation and induces apoptosis
629 in response to cerebral I/R injury (Ito et al., 2015). NF-κB is a vital transcription
630 factor and the initial signal for eliciting the NLRP3 inflammasome formation, whose
631 activity is mediated by IκB, an inhibitor of NF-κB (Zou et al., 2022). In unactivated
632 condition, NF-κB dimer binds to IκB in the cytoplasm. Upon simulation of
633 inflammatory response, IKK-α and- β, are the two catalytic subunits of the IKK, were
634 activated and then phosphorylate the IκB-bound-NF-κB protein complex, which
635 facilitates NF-κB nuclear translocation, and subsequently accelerates proinflammatory
636 factors release (Kwon et al., 2021). As expected, we found that TLB markedly
637 reduced cerebral I/R injury-induced proinflammatory factors via mediated NF-
638 κB/NLRP3 axis. Furthermore, MMP9 is a pivotal member of MMPs and enriched in
639 astrocytes and ECs, which is activated by NF-κB and injures TJs and basilar

640 membrane, resulting in BBB breakdown after cerebral I/R injury (B. Liu et al., 2021;
641 Medina-Flores et al., 2020). Recent studies have found that the proinflammatory
642 CypA/NF-κB/MMP9 pathway controls integrity of BBB, which requires APOE4
643 (Bell et al., 2012). APOE4 is an isoform of APOE that is enrichment in astrocytes,
644 resulting in chronic neuroinflammation (Tcw et al., 2022). Of note, APOE4
645 contributes to accelerated BBB disruption and deterioration of brain capillary
646 pericytes that sustain integrity of BBB in the pathology of Alzheimer's disease
647 (Arnaud et al., 2022). However, whether APOE4 is also an ischemic stroke
648 susceptibility gene is unclear. Intriguingly, we found that APOE4 protein expression
649 were significantly increased after cerebral I/R injury, which suggested that APOE4
650 also act as an important effector for mediation of BBB integrity in ischemic stroke.
651 whereas, TLB effectively reduced APOE4 following challenged by cerebral I/R injury.
652 Moreover, in keeping with theory that CypA at pathophysiological levels activates the
653 NF-κB/MMP9 pathway (Bell et al., 2012), we found that CypA and MMP9 protein
654 expressions were increased, and TIMP (an inhibitor of MMP9) protein expression was
655 decreased upon cerebral I/R stimuli; however, these changes were reversed by TLB,
656 which suggested that APOE4/CypA/NF-κB/MMP9 signaling pathway was involved
657 in the BBB protection of TLB on cerebral I/R injury.
658 Collectively, these findings suggested that TLB rescues BBB breakdown following
659 cerebral I/R insult, at least partly, through APOE4/CypA/NF-κB/MMP9 signaling
660 pathway, thereby inhibits inflammation and apoptosis, consisting with the results of
661 transcriptomics. Nevertheless, the detailed mechanism or potential targets are still

662 unclear and it deserves to be elucidated in-depth.

663 Subsequently, we predicted the possible underlying targets of TLB with the help of in
664 silico computational molecular docking. The results showed that TLB directly bound
665 to MMP9, but not APOE4, CypA and NF-κB. Combined with the results mentioned
666 above, we hypothesized that MMP9 might be the potential targets of TLB on cerebral
667 I/R injury-induced BBB breakdown. To test that hypothesis, we used OGD/R-induced
668 injury in co-cultured human BMVECs and astrocytes *in vitro* to mimic BBB
669 breakdown *in vivo*. Our data showed that TLB effectively inhibited OGD/R-induced
670 loss of cellular integrity and cell death in ECs, in line with the results in *in vivo*. Next,
671 to understand the contribution of MMP9 to the BBB protection of TLB, MMP9 gene
672 was silenced in OGD/R stimulated human BMVECs and astrocytes. The results
673 revealed that knockdown of MMP9 by siRNA substantially abolished the OGD/R-
674 induced injury in ECs, in consistent with the theory that MMP9 plays a vital role in
675 maintaining BBB integrity. Whereas, the protective effect of TLB on ECs after
676 OGD/R insult was markedly reinforced by knockdown of MMP9, which suggested
677 that MMP9 might be the potential target of TLB-evoked BBB protection.

678 In the present study, the findings extend our previous discovery of TLB protects
679 against cerebral I/R injury and present a novel target of TLB for salvation of BBB
680 breakdown. Intriguingly, our findings reveal that APOE4 maintains BBB integrity
681 essential for neurological function through mediating the CypA/NF-κB/MMP9
682 signaling pathway. We also found that MMP9 is a potential target of TLB for
683 combating APOE4-modulated BBB disruption in ischemic stroke. Notwithstanding

684 promotional experimental evidences, there are still limitations in this study. First,
685 despite we offer a directly evidence that TLB could maintain the BBB integrity after
686 cerebral I/R injury, whether TLB can penetrate BBB and what is the pharmacokinetic,
687 distribution and metabolism of TLB in the brain during ischemic stroke are blurry.
688 Second, whether TLB could hinder hemorrhagic transformation following BBB
689 breakdown is unclear. Finally, whether TLB impacts other mechanisms such as
690 autophagy, ferroptosis, pyroptosis after BBB disruption in ischemic stroke is also
691 unknown. In fact, these outstanding issues will be addressed in our next study.
692 In summary, our findings uncover that TLB confers robust protection aginst BBB
693 disruption after cerebral I/R injury by targeting MMP9 through mediating
694 APOE4/CypA/NF-κB axis. These findings suggest that TLB may be a powerful
695 weapon in conquering ischemic stroke and expands the probability of new tactics to
696 accomplish neuroprotection.

697 **References**

698 Abraham, M. J., Murtola, T., Schulz, R., Páll, S., & Lindahl, E. J. S. (2015).
699 GROMACS: high performance molecular simulations through multi-level
700 parallelism from laptops to supercomputers. Softwarex, 1-2(C), 19-25.
701 Arnaud, L., Benech, P., Greetham, L., Stephan, D., Jimenez, A., Jullien, N., … Nivet,
702 E. (2022). APOE4 drives inflammation in human astrocytes via TAGLN3
703 repression and NF-kappaB activation. Cell Rep, 40(7), 111200.
704 doi:10.1016/j.celrep.2022.111200
705 Bell, R. D., Winkler, E. A., Singh, I., Sagare, A. P., Deane, R., Wu, Z., … Zlokovic,

706 B. V. (2012). Apolipoprotein E controls cerebrovascular integrity via
707 cyclophilin A. Nature, 485(7399), 512-516. doi:10.1038/nature11087
708 Ben-Zvi, A., Lacoste, B., Kur, E., Andreone, B. J., Mayshar, Y., Yan, H., & Gu, C.
709 (2014). Mfsd2a is critical for the formation and function of the blood-brain
710 barrier. Nature, 509(7501), 507-511. doi:10.1038/nature13324
711 Cai, Y., Lu, X., Cheng, X., Lv, Q., Xu, G., & Liu, X. (2022). Increased renal
712 dysfunction, apoptosis, and fibrogenesis through sympathetic hyperactivity
713 after focal cerebral infarction. Transl Stroke Res, 13(4), 641-651.
714 doi:10.1007/s12975-021-00900-w
715 Calderon, M. R., Mori, M., Kauwe, G., Farnsworth, J., Ulian-Benitez, S., Maksoud,
716 E., … Haghighi, A. P. (2022). Delta/Notch signaling in glia maintains motor
717 nerve barrier function and synaptic transmission by controlling matrix
718 metalloproteinase expression. Proc Natl Acad Sci U S A, 119(34),
719 e2110097119. doi:10.1073/pnas.2110097119
720 Chang, J., Mancuso, M. R., Maier, C., Liang, X., Yuki, K., Yang, L., … Kuo, C. J.
721 (2017). Gpr124 is essential for blood-brain barrier integrity in central nervous
722 system disease. Nat Med, 23(4), 450-460. doi:10.1038/nm.4309
723 Chen, H., Guan, B., Chen, S., Yang, D., & Shen, J. (2021). Peroxynitrite activates
724 NLRP3 inflammasome and contributes to hemorrhagic transformation and
725 poor outcome in ischemic stroke with hyperglycemia. Free Radic Biol Med,
726 165, 171-183. doi:10.1016/j.freeradbiomed.2021.01.030
727 Chen, N., Wang, J., He, Y., Xu, Y., Zhang, Y., Gong, Q., … Gao, J. (2020).

728 Trilobatin protects against abeta25-35-induced hippocampal HT22 cells
729 apoptosis through mediating ROS/p38/Caspase 3-dependent pathway. Front
730 Pharmacol, 11, 584. doi:10.3389/fphar.2020.00584
731 Chen, X., Zhang, J., & Wang, K. (2022). Inhibition of intracellular proton-sensitive
732 Ca(2+)-permeable TRPV3 channels protects against ischemic brain injury.
733 Acta Pharm Sin B, 12(5), 2330-2347. doi:10.1016/j.apsb.2022.01.001
734 Curtis, M. J., Ashton, J. C., Moon, L. D. F., & Ahluwalia, A. (2018). Clarification of
735 the basis for the selection of requirements for publication in the British Journal
736 of Pharmacology. Br J Pharmacol, 175(18), 3633-3635.
737 doi:10.1111/bph.14443
738 Fan, X., Zhang, Y., Dong, H., Wang, B., Ji, H., & Liu, X. (2015). Trilobatin
739 attenuates the LPS-mediated inflammatory response by suppressing the NF-
740 kappaB signaling pathway. Food Chem, 166, 609-615.
741 doi:10.1016/j.foodchem.2014.06.022
742 Fischer, U., Kaesmacher, J., Strbian, D., Eker, O., Cognard, C., Plattner, P. S., …
743 Collaborators, S. D. (2022). Thrombectomy alone versus intravenous alteplase
744 plus thrombectomy in patients with stroke: an open-label, blinded-outcome,
745 randomised non-inferiority trial. Lancet, 400(10346), 104-115.
746 doi:10.1016/S0140-6736(22)00537-2
747 Gao, J., Chen, N., Li, N., Xu, F., Wang, W., Lei, Y., … Gong, Q. (2020).
748 Neuroprotective effects of trilobatin, a novel naturally occurring Sirt3 agonist
749 from lithocarpus polystachyus rehd., mitigate cerebral ischemia/reperfusion

750 injury: involvement of TLR4/NF-kappaB and Nrf2/Keap-1 signaling. Antioxid
751 Redox Signal, 33(2), 117-143. doi:10.1089/ars.2019.7825
752 Gao, J., Liu, S., Xu, F., Liu, Y., Lv, C., Deng, Y., … Gong, Q. (2018). Trilobatin
753 protects against oxidative injury in neuronal PC12 cells through regulating
754 mitochondrial ROS homeostasis mediated by AMPK/Nrf2/Sirt3 signaling
755 pathway. Front Mol Neurosci, 11, 267. doi:10.3389/fnmol.2018.00267
756 Gao, J., Long, L., Xu, F., Feng, L., Liu, Y., Shi, J., & Gong, Q. (2020). Icariside II, a
757 phosphodiesterase 5 inhibitor, attenuates cerebral ischaemia/reperfusion injury
758 by inhibiting glycogen synthase kinase-3beta-mediated activation of
759 autophagy. Br J Pharmacol, 177(6), 1434-1452. doi:10.1111/bph.14912
760 Gao, J. M., Zhang, X., Shu, G. T., Chen, N. N., Zhang, J. Y., Xu, F., … Gong, Q. H.
761 (2022). Trilobatin rescues cognitive impairment of Alzheimer's disease by
762 targeting HMGB1 through mediating SIRT3/SOD2 signaling pathway. Acta
763 Pharmacol Sindoi:10.1038/s41401-022-00888-5
764 Gong, S., Cao, G., Li, F., Chen, Z., Pan, X., Ma, H., … Kou, J. (2021). Endothelial
765 conditional knockdown of NMMHC IIA (nonmuscle myosin heavy chain IIA)
766 attenuates blood-brain barrier damage during Ischemia-reperfusion injury.
767 Stroke, 52(3), 1053-1064. doi:10.1161/STROKEAHA.120.031410
768 Iorio, R., Celenza, G., & Petricca, S. (2022). Multi-target effects of ß-caryophyllene
769 and carnosic acid at the crossroads of mitochondrial dysfunction and
770 neurodegeneration: from oxidative stress to microglia-mediated
771 neuroinflammation. Antioxidants (Basel), 11(6)doi:10.3390/antiox11061199

772 Ito, M., Shichita, T., Okada, M., Komine, R., Noguchi, Y., Yoshimura, A., & Morita,
773 R. (2015). Bruton's tyrosine kinase is essential for NLRP3 inflammasome
774 activation and contributes to ischaemic brain injury. Nat Commun, 6, 7360.
775 doi:10.1038/ncomms8360
776 Khalifa, A. A., El Sokkary, N. H., Elblehi, S. S., Diab, M. A., & Ali, M. A. (2022).
777 Potential cardioprotective effect of octreotide via NOXs mitigation,
778 mitochondrial biogenesis and MAPK/Erk1/2/STAT3/NF-kbeta pathway
779 attenuation in isoproterenol-induced myocardial infarction in rats. Eur J
780 Pharmacol, 925, 174978. doi:10.1016/j.ejphar.2022.174978
781 Kilkenny, C., Browne, W., Cuthill, I. C., Emerson, M., Altman, D. G., & Group, N. C.
782 R. R. G. W. (2010). Animal research: reporting in vivo experiments: the
783 ARRIVE guidelines. Br J Pharmacol, 160(7), 1577-1579. doi:10.1111/j.1476-
784 5381.2010.00872.x
785 Kim, Y. Y., Hur, G., Lee, S. W., Lee, S. J., Lee, S., Kim, S. H., & Rho, M. C. (2020).
786 AGK2 ameliorates mast cell-mediated allergic airway inflammation and
787 fibrosis by inhibiting FcepsilonRI/TGF-beta signaling pathway. Pharmacol
788 Res, 159, 105027. doi:10.1016/j.phrs.2020.105027
789 Kwon, O. C., Song, J. J., Yang, Y., Kim, S. H., Kim, J. Y., Seok, M. J., … Lee, S. H.
790 (2021). SGK1 inhibition in glia ameliorates pathologies and symptoms in
791 Parkinson disease animal models. EMBO Mol Med, 13(4), e13076.
792 doi:10.15252/emmm.202013076
793 Lama, A., Pirozzi, C., Severi, I., Morgese, M. G., Senzacqua, M., Annunziata, C., …

794 Meli, R. (2022). Palmitoylethanolamide dampens neuroinflammation and
795 anxiety-like behavior in obese mice. Brain Behav Immun, 102, 110-123.
796 doi:10.1016/j.bbi.2022.02.008
797 Lei, T., Yang, Z., Xia, X., Chen, Y., Yang, X., Xie, R., … Gao, H. (2021). A
798 nanocleaner specifically penetrates the bloodbrain barrier at lesions to clean
799 toxic proteins and regulate inflammation in Alzheimer's disease. Acta Pharm
800 Sin B, 11(12), 4032-4044. doi:10.1016/j.apsb.2021.04.022
801 Liu, B., Li, Y., Han, Y., Wang, S., Yang, H., Zhao, Y., … Wang, Y. (2021).
802 Notoginsenoside R1 intervenes degradation and redistribution of tight
803 junctions to ameliorate blood-brain barrier permeability by Caveolin-
804 1/MMP2/9 pathway after acute ischemic stroke. Phytomedicine, 90, 153660.
805 doi:10.1016/j.phymed.2021.153660
806 Liu, L., Yang, C., Lavayen, B. P., Tishko, R. J., Larochelle, J., & Candelario-Jalil, E.
807 (2022). Targeted BRD4 protein degradation by dBET1 ameliorates acute
808 ischemic brain injury and improves functional outcomes associated with
809 reduced neuroinflammation and oxidative stress and preservation of blood-
810 brain barrier integrity. J Neuroinflammation, 19(1), 168. doi:10.1186/s12974-
811 022-02533-8
812 Liu, M. B., Wang, W., Gao, J. M., Li, F., Shi, J. S., & Gong, Q. H. (2020). Icariside II
813 attenuates cerebral ischemia/reperfusion-induced blood-brain barrier
814 dysfunction in rats via regulating the balance of MMP9/TIMP1. Acta
815 Pharmacol Sin, 41(12), 1547-1556. doi:10.1038/s41401-020-0409-3

816 Matei, N., Camara, J., McBride, D., Camara, R., Xu, N., Tang, J., & Zhang, J. H.
817 (2018). Intranasal wnt3a attenuates neuronal apoptosis through
818 Frz1/PIWIL1a/FOXM1 pathway in MCAO rats. J Neurosci, 38(30), 6787-
819 6801. doi:10.1523/JNEUROSCI.2352-17.2018
820 McGrath, J. C., Drummond, G. B., McLachlan, E. M., Kilkenny, C., & Wainwright, C.
821 L. (2010). Guidelines for reporting experiments involving animals: the
822 ARRIVE guidelines. British Journal of Pharmacology, 160(7), 1573-1576.
823 doi:10.1111/j.1476-5381.2010.00873.x
824 Medina-Flores, F., Hurtado-Alvarado, G., Contis-Montes de Oca, A., Lopez-
825 Cervantes, S. P., Konigsberg, M., Deli, M. A., & Gomez-Gonzalez, B. (2020).
826 Sleep loss disrupts pericyte-brain endothelial cell interactions impairing blood-
827 brain barrier function. Brain Behav Immun, 89, 118-132.
828 doi:10.1016/j.bbi.2020.05.077
829 Montagne, A., Nation, D. A., & Zlokovic, B. V. (2020). APOE4 accelerates
830 development of dementia after stroke: is tthere a role for cerebrovascular
831 dysfunction? Stroke, 51(3), 699-700. doi:10.1161/STROKEAHA.119.028814
832 Mora, P., Hollier, P. L., Guimbal, S., Abelanet, A., Diop, A., Cornuault, L., …
833 Chapouly, C. (2020). Blood-brain barrier genetic disruption leads to protective
834 barrier formation at the glia limitans. PLoS Biol, 18(11), e3000946.
835 doi:10.1371/journal.pbio.3000946
836 Ng, F. C., Churilov, L., Yassi, N., Kleinig, T. J., Thijs, V., Wu, T. Y., … Investigators.
837 (2022). Microvascular dysfunction in blood-brain barrier disruption and

838 hypoperfusion within the infarct posttreatment are associated with cerebral
839 edema. Stroke, 53(5), 1597-1605. doi:10.1161/STROKEAHA.121.036104
840 Nikolakopoulou, A. M., Wang, Y., Ma, Q., Sagare, A. P., Montagne, A., Huuskonen,
841 M. T., … Zlokovic, B. V. (2021). Endothelial LRP1 protects against
842 neurodegeneration by blocking cyclophilin A. J Exp Med,
843 218(4)doi:10.1084/jem.20202207
844 Palomino-Antolin, A., Narros-Fernandez, P., Farre-Alins, V., Sevilla-Montero, J.,
845 Decouty-Perez, C., Lopez-Rodriguez, A. B., … Egea, J. (2022). Time-
846 dependent dual effect of NLRP3 inflammasome in brain ischaemia. Br J
847 Pharmacol, 179(7), 1395-1410. doi:10.1111/bph.15732
848 Ren, N., Ogata, S., Kiyoshige, E., Nishimura, K., Nishimura, A., Matsuo, R., … The
849 Gap-Stroke, J. S. C. (2022). Associations between adherence to evidence-
850 based, stroke quality indicators and outcomes of acute reperfusion therapy.
851 Stroke, 53, 00-00. doi:10.1161/STROKEAHA.121.038483
852 Richter, A., Lange, S., Holz, C., Brock, L., Freitag, T., Sekora, A., … Junghanss, C.
853 (2022). Effective tumor cell abrogation via Venetoclax-mediated BCL-2
854 inhibition in KMT2A-rearranged acute B-lymphoblastic leukemia. Cell Death
855 Discov, 8(1), 302. doi:10.1038/s41420-022-01093-3
856 Shang, A., Liu, H. Y., Luo, M., Xia, Y., Yang, X., Li, H. Y., … Gan, R. Y. (2022).
857 Sweet tea (Lithocarpus polystachyus rehd.) as a new natural source of
858 bioactive dihydrochalcones with multiple health benefits. Crit Rev Food Sci
859 Nutr, 62(4), 917-934. doi:10.1080/10408398.2020.1830363

860 Tcw, J., Qian, L., Pipalia, N. H., Chao, M. J., Liang, S. A., Shi, Y., … Goate, A. M.
861 (2022). Cholesterol and matrisome pathways dysregulated in astrocytes and
862 microglia. Cell, 185(13), 2213-2233 e2225. doi:10.1016/j.cell.2022.05.017
863 Van Der Spoel, D., Lindahl, E., Hess, B., Groenhof, G., Mark, A. E., & Berendsen, H.
864 J. C. (2005). GROMACS: fast, flexible, and free. Journal of Computational
865 Chemistry, 26(16), 1701-1718. doi:10.1002/jcc.20291
866 Xiao, R., Wei, Y., Zhang, Y., Xu, F., Ma, C., Gong, Q., … Xu, Y. (2022). Trilobatin,
867 a naturally occurring food additive, ameliorates exhaustive exercise-induced
868 fatigue in mice: involvement of Nrf2/ARE/Ferroptosis signaling pathway.
869 Front Pharmacol, 13, 913367. doi:10.3389/fphar.2022.913367
870 Yang, T., Sun, Y., Mao, L., Zhang, M., Li, Q., Zhang, L., … Zhang, F. (2018). Brain
871 ischemic preconditioning protects against ischemic injury and preserves the
872 blood-brain barrier via oxidative signaling and Nrf2 activation. Redox Biol, 17,
873 323-337. doi:10.1016/j.redox.2018.05.001
874 Yang, Z., Gao, Z., Yang, Z., Zhang, Y., Chen, H., Yang, X., … Chu, L. (2022).
875 Lactobacillus plantarum-derived extracellular vesicles protect against ischemic
876 brain injury via the microRNA-101a-3p/c-Fos/TGF-beta axis. Pharmacol Res,
877 182, 106332. doi:10.1016/j.phrs.2022.106332
878 Yu, L., Liu, S., Zhou, R., Sun, H., Su, X., Liu, Q., … Qu, Y. (2022). Atorvastatin
879 inhibits neuronal apoptosis via activating cAMP/PKA/p-CREB/BDNF
880 pathway in hypoxic-ischemic neonatal rats. FASEB J, 36(4), e22263.
881 doi:10.1096/fj.202101654RR

882 Zheng, Y., Deng, Y., Gao, J. M., Lv, C., Lang, L. H., Shi, J. S., … Gong, Q. H.
883 (2020). Icariside II inhibits lipopolysaccharide-induced inflammation and
884 amyloid production in rat astrocytes by regulating IKK/IkappaB/NF-
885 kappaB/BACE1 signaling pathway. Acta Pharmacol Sin, 41(2), 154-162.
886 doi:10.1038/s41401-019-0300-2
887 Zou, Y., Zhang, M., Wu, Q., Zhao, N., Chen, M., Yang, C., … Han, B. (2022).
888 Activation of transient receptor potential vanilloid 4 is involved in pressure
889 overload-induced cardiac hypertrophy. Elife, 11doi:10.7554/eLife.74519

890 **Figure legends**

891 **Fig. 1 TLB protected against BBB disruption after cerebral I/R injury in rats.** a.
892 Perfusion and oxygenation imager showed that regional cerebral blood flow (rCBF) in
893 MCAO model decreased to 20% and recovered to 80% of baseline. b. Quantitation of
894 rCBF (n = 6). c. Neurological deficits scores (n = 6). d. Representative images of
895 TTC-stained brain sections at Day 3. e. Quantification of infarct volume at Day 3 (n
896 = 6). f. Representative images of EB leakage dye. g. Quantification of extravasated
897 EB leakage dye (n = 6). h. Ultrastructural changes were observed by TEM. Cap
898 (×40,000, scale bar = 500 nm), neurons (yellow arrow) and MS (red arrow) (×15,000,
899 scale bar = 2 μm). Data are presented as mean ± SD. $^{*}P < 0.05$ *versus* sham group; $^{\#}P$
900 < 0.05 *versus* MCAO group.

901 **Fig. 2 TLB suppressed injury to the hippocampus, striatum and cortex after**
902 **cerebral I/R injury in rats and molecular docking analysis.** a. Representative
903 images of HE staining in the hippocampus, striatum, and cortex (×400, scale bar = 50
904 μm, n = 6). b. The DEGs between MCAO versus sham group and MCAO versus

905 MCAO + TLB group. c. Enrichment analyses were performed using David showing
906 biological processes (GO) to predict changes. d. The top 10 KEGG pathways enriched
907 in DEGs and their corresponding *P*-values. e. PPI network of DEGs resulting from
908 TLB treatment of I/R injury in rats. The size of the node is related to the importance
909 of the node, with larger nodes MMP9 sharing more connections to other nodes.
910 **Fig. 3 TLB protected against cerebral I/R injury-induced loss of neurons and TJ**
911 **proteins in rats.** a. The major cellular components of BBB were displayed in the
912 scheme. b. Representative images of Nissl staining in hippocampus and cortex. c.
913 Nissl-positive neurons in CA1 region (n = 6). d. Nissl-positive neurons in CA3 region
914 (n = 6). e. Nissl-positive neurons in DG region (n = 6). f. Nissl-positive neurons in the
915 cortex (n = 6). g. Representative Western blot of ZO-1 protein expressions. h.
916 Quantitation of ZO-1 protein (n = 6). i. Representative Western blot of claudin 5
917 protein expressions. j. Quantitation of claudin 5 protein (n = 6). k. Representative
918 Western blot of occludin protein expressions. l. Quantitation of occludin protein (n =
919 6). Data are presented as mean ± SD. $^{*}P < 0.05$ *versus* sham group; $^{\#}P < 0.05$ *versus*
920 MCAO group.
921 **Fig. 4 TLB modulated TIMP1/MMP9 balance and suppressed APOE4/CypA**
922 **signaling pathway after cerebral I/R injury.** a. Representative image of MMP9
923 expression in the cortex and striatum by IHC. b. Quantitation of MMP9 in the
924 striatum (n = 6). c. Quantitation of MMP9 in the cortex (n = 6). d. Representative
925 Western blot of MMP9. e. Quantification of MMP9 protein expression (n = 6). f.
926 Representative image by gelatin zymography. g. Quantification of activity of MMP9
927 (n = 6). h. Representative images of TIMP1 in the cortex and striatum by IHC. i.

928 Quantitation of TIMP1 in the striatum (n = 6). j. Quantitation of TIMP1 in the cortex
929 (n = 6). k. Representative Western blot of TIMP1 protein expression. l. Quantification
930 of TIMP1 protein expression (n = 6). m. Representative Western blot of APOE4
931 protein expression. n. Quantification of APOE4 protein expression (n = 6). o.
932 Representative Western blot of CypA protein expression. p. Quantitation of CypA
933 protein expression (n = 6). Data are presented as mean ± SD. $^{*}P < 0.05$ *versus* sham
934 group; $^{\#}P < 0.05$ *versus* MCAO group.

935 **Fig. 5 TLB suppressed neuroinflammation through inhibiting NF-κB signaling**
936 **pathway after cerebral I/R insult in rats.** a. IL-1β (n = 6). b. IL-6 (n = 6). c. IL-4 (n
937 = 6). d. IL-10 (n = 6). e. Representative Western blots of IκB-α protein expression. f.
938 Quantitation of IκB-α protein expression (n = 6). g. Representative Western blots of
939 p-IKK-α protein expression. h. Quantitation of p-IKK-α protein level (n = 6). i.
940 Representative Western blots of p-IKK-β. j. Quantitation of p-IKK-β protein level (n
941 = 6). k. Representative Western blots of p-NF-κBp65 protein level. l. Quantitation of
942 p-NF-κBp65 protein level (n = 6). m. Representative Western blots of NLRP3 protein.
943 n. Quantitation of NLRP3 protein expression (n = 6). Data are presented as mean ±
944 SD. $^{*}P < 0.05$ *versus* sham group; $^{\#}P < 0.05$ *versus* MCAO group.

945 **Fig. 6 TLB suppresses neuronal death through inhibiting caspase 3-dependent**
946 **apoptosis pathway after cerebral I/R injury in rats.** a. Representative images of
947 TUNEL staining in the hippocampus and cortex. b. Quantitation of TUNEL-positive
948 cells in CA1 region of hippocampus (n = 6). c. Quantitation of TUNEL-positive cells
949 in CA3 region of hippocampus (n = 6). d. Quantitation of TUNEL-positive cells in
950 DG region of hippocampus (n = 6). e. Quantitation of TUNEL-positive cells in cortex
951 (n = 6). f. Representative Western blots of Bax and Bcl-2 protein expressions. g. The
952 ratio of Bax/Bcl-2 (n = 6). h. Representative Western blots of cleaved-caspase 3 level

953 and caspase 3 protein expression. i. Quantitation of cleaved-caspase 3/caspase 3 (n =
954 6). Data are presented as mean ± SD. $^{*}P < 0.05$ *versus* sham group; $^{\#}P < 0.05$ *versus*
955 MCAO group.

956 **Fig. 7 TLB inhibited loss of BBB integrity through activating**
957 **APOE4/CypA/MMP9 signaling pathway after OGD/R insult in human**
958 **BMEC/astrocytes co-cultures.** Human BMEC/astrocytes co-cultures were treated
959 with TLB or PH002 for 24 h upon OGD/R. a. Scheme. b. TEER value (n = 6). c.
960 Representative images of Live/Dead staining. d. Quantitation of Live/Dead staining
961 (n = 6). Live cells were presented as green and dead cells were presented as red (×40,
962 scale bar = 500 μm). e. LDH leakage (n = 6). f. Representative Western blot of
963 APOE4, CypA and MMP9 protein expressions. g. Quantitation of APOE4 protein
964 expression (n = 6). h. Quantitation of CypA protein expression (n = 6). i. Quantitation
965 of MMP9 protein expression (n = 6). Data are presented as mean ± SD. $^{*}P < 0.05$
966 *versus* Control group; $^{\#}P < 0.05$ *versus* OGD/R group; $^{\blacktriangle}P < 0.05$ *versus* OGD/R +
967 TLB 50 group.

968 **Fig. 8 TLB directly bound to MMP9.** a. Model structures presented the complex
969 formed by the MMP9 ligand-binding pocket and TLB by in silico computational
970 molecular docking. MD process using the GROMACS 4.6.6 simulation protocol. b.
971 Gibbs energy lanscape of the TLB-MMP9 compound complex. The color scale
972 diagram shows the gibbs energy profile (kcal/mol) and the dark blue profile is the
973 minimum depth. c. Gibbs energy landscape profile of TLB-MMP9 complex. d. The
974 RMSD of the TLB-MMP9 complex with respect to its initial structure as a function of
975 time. e. RMSF of residues of the whole protein in the TLB-MMP9 complex and free
976 MMP9 during the 100000 ps.

977 **Fig. 9 TLB protect against OGD/ R-induced damage of blood-brain barrier**

978 **integrity by blocking MMP9.** a. Scheme. b. TEER value (n = 6). c. Representative

979 images of Live/Dead staining. d. Quantitation of Live/Dead staining (n = 6). Live

980 cells were presented as green and dead cells were presented as red (×40, scale bar =

981 500 μm). e. LDH leakage (n = 6). Data are presented as mean ± SD. $^{*}P < 0.05$ *versus*

982 Control group; $^{\#}P < 0.05$ *versus* OGD/R group; $^{\blacktriangle}P < 0.05$ *versus* OGD/R + TLB 50

983 group; $^{\$}P < 0.05$ *versus* OGD/R + siMMP9 group.

984 **Fig. 10 Schematic diagram illustrating a potential mechanism for the protective**

985 **role of TLB on BBB disruption after cerebral I/R injury.** TLB effectively rescues

986 BBB breakdown, reduces inflammation and apoptosis. TLB interacts with MMP9 and

987 through mediating APOE4/CypA/NF-κB axis to confer BBB neuroprotection.